First Principles Quantum Dynamical Investigation Provides Evidence for the Role of Polycyclic Aromatic Hydrocarbon Radical Cations in Interstellar Physics

V. Sivaranjana Reddy, S. Ghanta, and S. Mahapatra*

School of Chemistry & ACRHEM, University of Hyderabad, Hyderabad 500 046, India

(Received 4 November 2009; published 19 March 2010)

Inspired by the recent astronomical discovery of new diffused interstellar bands (DIBs) assigned to the electronic transitions in the naphthalene radical cation based on complementary laboratory measurements, we attempt here an *ab initio* quantum dynamical study to validate this assignment. In addition, the existence and mechanistic details of nonradiative deactivation of electronically excited polycyclic aromatic hydrocarbon (PAH) radical cations in the interstellar medium and their identity as carriers of DIBs are established here focusing on the prototypical naphthalene and anthracene radical cations of the PAH family.

DOI: 10.1103/PhysRevLett.104.111102 PACS numbers: 95.30.Ky, 31.15.−p

Understanding the origin of diffused interstellar bands (DIBs) and their assignments is a long-standing issue in astrophysical investigations [1]. The consensus is that they originate from electronically excited radical cations of polycyclic aromatic hydrocarbons (PAHs), most abundant in the interstellar medium (ISM) [2]. This PAH hypothesis inspired new laboratory measurements in the typical conditions of ISM which revealed diffuse vibronic bands and subpicosecond dynamics of their low-lying electronic states [3–10]. Very recently, spectroscopic measurements of the star Cernis 52 located in the Perseus molecular cloud led to the discovery of three new DIBs [11]. Aided by laboratory measurements, they are assigned to electronic transitions in the naphthalene radical cation (NP^+). Despite some attempts [12,13] a detailed complementary theoretical study is still missing.

We attempt here a theoretical study on the prototypical members, viz., NP^+ and anthracene radical cation (AN^+) of the PAH family. Our efforts are driven by desires to (1) complement the assignment of the new DIBs and (2) understand the underlying mechanism of subpicosecond decay, broad vibronic bands, and photostability of PAH cations. We address that a detailed *ab initio* quantum dynamical treatment of these systems is handicapped by their large number of electronic and nuclear degrees of freedom (DOF). These are often strongly coupled and the approach necessarily goes beyond the adiabatic Born-Oppenheimer (BO) framework [14]. A coupling between electronic and nuclear DOF leads to strong nonadiabaticity and complex mechanisms for the charge and energy transfer in these systems.

Our approach here is based on a diabatic electronic basis (to avoid singular nonadiabatic coupling of the adiabatic electronic basis) and *ab initio* calculations of the potential energy surfaces (PESs) to describe the quantum dynamics of six low-lying coupled electronic states of NP^+ and AN^+ created upon photoionization of their neutrals. A vibronic Hamiltonian pertaining to this situation is given by [15]

$$\mathcal{H} = (\mathcal{T}_N + \mathcal{V}_0)\mathbf{I_6} + \Delta\mathcal{H}, \tag{1}$$

where $\mathcal{T}_N$ and $\mathcal{V}_0$ describe the nuclear and electronic parts, respectively, of the Hamiltonian of the reference electronic ground state of neutral naphthalene (NP) or anthracene (AN). This reference state is assumed to be vibronically decoupled from the other states and nuclear motion in it is treated as harmonic. $\mathbf{I_6}$ represents a 6×6 unit matrix. The quantity $\Delta\mathcal{H}$ (the change in electronic energy upon ionization) is given by

$$\Delta\mathcal{H} = \begin{pmatrix} W_{\tilde{X}} & W_{\tilde{X}-\tilde{A}} & W_{\tilde{X}-\tilde{B}} & W_{\tilde{X}-\tilde{C}} & W_{\tilde{X}-\tilde{D}} & W_{\tilde{X}-\tilde{E}} \\ & W_{\tilde{A}} & W_{\tilde{A}-\tilde{B}} & W_{\tilde{A}-\tilde{C}} & W_{\tilde{A}-\tilde{D}} & W_{\tilde{A}-\tilde{E}} \\ & & W_{\tilde{B}} & W_{\tilde{B}-\tilde{C}} & W_{\tilde{B}-\tilde{D}} & W_{\tilde{B}-\tilde{E}} \\ \text{H.c.} & & & W_{\tilde{C}} & W_{\tilde{C}-\tilde{D}} & W_{\tilde{C}-\tilde{E}} \\ & & & & W_{\tilde{D}} & W_{\tilde{D}-\tilde{E}} \\ & & & & & W_{\tilde{E}} \end{pmatrix}. \tag{2}$$

In the above, the diagonal and off-diagonal elements refer to the energy of the diabatic electronic and their coupling surfaces, respectively. Employing dimensionless normal displacement coordinates (Q) of vibrational modes of the reference state, using a standard Taylor series expansion around the reference geometry (at $\mathbf{Q} = 0$) and symmetry selection rule these are given by

$$W_j = E_0^{(j)} + \sum_{i \in \nu_{a_g}} \kappa_i^{(j)} Q_i + \frac{1}{2} \sum_{i \in \nu_{\text{all}}} \gamma_i^{(j)} Q_i^2 + \ldots. \tag{3}$$

$$W_{j-k} = \sum_{i \in \nu_c} \lambda_i^{(j,k)} Q_i + \ldots. \tag{4}$$

In these equations, the quantity $E_0^{(j)}$ denotes the vertical ionization energy (VIE) of the jth electronic state. $\kappa_i^{(j)}$ represents the gradient along the totally symmetric vibrational modes ν_{a_g} and $\gamma_i^{(j)}$ represents the curvature along all vibrational modes of the jth electronic state at $\mathbf{Q} = 0$. The quantity $\lambda^{(j,k)}$ represents the coupling parameter along the coupling mode ν_c between the electronic states j and k.

The dynamical observables are recorded in terms of eigenvalue spectrum and decay rate of excited electronic states. Although a time-independent solution of the eigenvalue equation yields precise location of vibronic levels, it becomes prohibitively difficult for systems with large DOF. A wave packet (WP) propagation approach within the multiconfiguration time-dependent Hartree (MCTDH) scheme [16] employed here appears to be the best alternative in this situation. The multiset ansatz of the MCTDH scheme allows a combination of vibrational DOF and an effective reduction of the dimensionality problem. The spectral intensity can be written as [17]

$$P(E) \approx 2\,\mathrm{Re}\int_0^\infty e^{iEt/\hbar}\langle\Psi(0)|e^{-i\mathcal{H}t/\hbar}|\Psi(0)\rangle dt, \qquad (5)$$

where $|\Psi(0)\rangle = |\Psi(t=0)\rangle = \boldsymbol{\tau}|\Psi^i\rangle$ is the initial WP ($|\Psi^i\rangle$) launched at the (final) electronic state of the radical cation. Elements of the transition dipole matrix $\boldsymbol{\tau}$ between the bound and scattering states are treated as constants of equal modulus utilizing the generalized Condon approximation [15]. An *ab initio* computation of these elements is highly cumbersome and techniques are lacking [18]. The highly oscillatory wave function of the outgoing electron possesses very small components in the Franck-Condon region. Previous studies with this approximation of branching ratios have given results in excellent agreement with the experiment indicating its reliability [15,17–19].

Both NP and AN possess D_{2h} equilibrium symmetry at their electronic ground state ($\tilde{X}^1A_g$). The symmetry representation of their vibrational modes is given by

$$\Gamma_{\mathrm{vib}} = 9(12)a_g + 4(5)a_u + 3(4)b_{1g} + 8(11)b_{1u} + 4(6)b_{2g} + 8(11)b_{2u} + 8(11)b_{3g} + 4(6)b_{3u} \quad \text{for } NP(AN). \qquad (6)$$

The low-lying six electronic states of NP^+ (AN^+), resulting from ionization from first six valence molecular orbitals of the reference state belong to $\tilde{X}^2A_u$ ($\tilde{X}^2B_{2g}$), $\tilde{A}^2B_{3u}$ ($\tilde{A}^2B_{1g}$), $\tilde{B}^2B_{2g}$ ($\tilde{B}^2A_u$), $\tilde{C}^2B_{1g}$ ($\tilde{C}^2B_{2g}$), $\tilde{D}^2A_g$ ($\tilde{D}^2B_{3u}$), and $\tilde{E}^2B_{3g}$ ($\tilde{E}^2A_g$) symmetry species. The symmetry rule allows a coupling of these states through (suitable) available vibrational modes of Eq. (6). The parameters κ_i, γ_i, and λ_i of Eqs. (3) and (4) are derived by performing extensive *ab initio* calculations of electronic energies along all 48 (66) vibrational modes of NP (AN). VIEs are calculated by the outer valence Green's function method [20,21] along Q_i. Including the reference state energies these are fitted to the diagonal adiabatic form of the diabatic Hamiltonian of Eq. (2) to estimate the parameters. A critical analysis of the parameters reveals that only 29 (31) vibrational modes are relevant for the nuclear dynamics in NP^+ (AN^+).

One-dimensional cuts of the multidimensional electronic PESs are shown typically in Figs. 1(a) and 1(b), along the important inter-ring symmetric C = C stretching mode of frequency ~1624 cm^{-1} (~ 1601 cm^{-1}) in NP (AN). It can be seen that for both NP^+ [panel (a)] and AN^+ [panel (b)], all six electronic states undergo numerous curve crossings. These crossings develop into conical intersections (CIs) in multidimensional vibrational space. Employing a linear coupling approach [15] various energetic minima of the PESs of NP^+ (AN^+) are estimated and given in Table I. The importance of these energy data in the nuclear dynamics is discussed below.

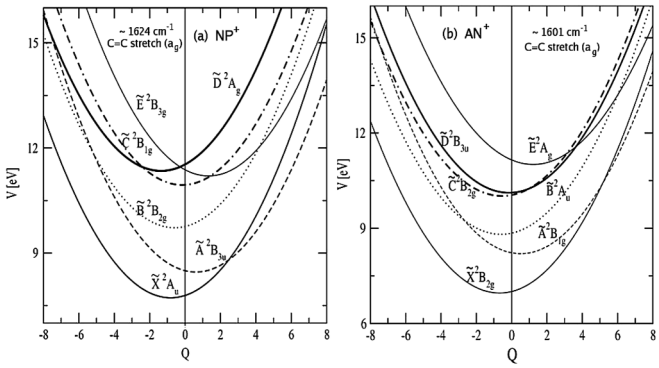

FIG. 1. Adiabatic potential energies of the $\tilde{X}$, $\tilde{A}$, $\tilde{B}$, $\tilde{C}$, $\tilde{D}$, and $\tilde{E}$ states of NP^+ [panel (a)] and AN^+ [panel (b)] along the symmetric C = C stretching vibration.

First principles simulations of nuclear dynamics are carried out on the coupled manifold of six electronic states including 29 (31) vibrational DOFs of NP^+ (AN^+). Six calculations are performed by launching the WP initially on each state separately. The WP is effectively propagated for a total of ~400 fs. The spectrum calculated using Eq. (5) from each propagation is combined to describe the composite vibronic structure of six electronic states. The results reveal resolved bands for the $\tilde{X}$, $\tilde{A}$, and $\tilde{B}$ and highly overlapping bands for the $\tilde{C}$-$\tilde{D}$-$\tilde{E}$ electronic states. The results are in good accord with the available photoelectron spectroscopy data [9,10]. A detailed presentation of the theoretical data is out of the scope of this Letter; we therefore focus on the important results that provide an understanding of recent novel astrophysical discovery.

The $\tilde{B}$ band of NP^+ has been the subject of major interest. Laboratory recordings of $D_0(\tilde{X}) \rightarrow D_2(\tilde{B})$ and $D_0(\tilde{X}) \rightarrow D_3(\tilde{C})$ transitions are also available [3–6]. The observed peaks are used recently to assign the three new DIBs [11]. So far no theoretical data are available to validate this assignment. The $\tilde{B}$ band of NP^+ is presented in Fig. 2(a) along with experimental results [9]. The agreement between the two is excellent. We performed several reduced-dimensional calculations via a matrix diagonalization method [15]. The results show the $\tilde{X}$-$\tilde{B}$ and $\tilde{B}$-$\tilde{C}$ couplings do not have much effect, however, the $\tilde{A}$-$\tilde{B}$ coupling causes a clustering of vibronic lines starting from the origin of the $\tilde{B}$ band. The calculated stick spectrum is included in the bottom panel of Fig. 2(a). Along with the progression of ~514 cm^{-1}, ~1458 cm^{-1} a_g vibrations, excitation of nontotally symmetric vibrations (for example, ~1636 cm^{-1} of b_{3u} symmetry) is also induced by this coupling. This results in a broadening of each peak.

TABLE I. Equilibrium minimum (diagonal entries) and minimum of the seam of various CIs (off-diagonal entries) of the PESs of NP^+ (AN^+). All quantities are given in eV.

	$\tilde{X}$	$\tilde{A}$	$\tilde{B}$	$\tilde{C}$	$\tilde{D}$	$\tilde{E}$
$\tilde{X}$	⋯	8.48(8.82)	13.67(15.44)	25.25(22.60)	14.38(30.90)	16.89(17.03)
$\tilde{A}$		8.37(8.10)	10.11(8.86)	20.94(11.59)	14.02(15.65)	13.50(15.06)
$\tilde{B}$			9.63(8.76)	11.64(12.55)	11.34(11.29)	12.07(12.31)
$\tilde{C}$				10.82(9.94)	11.08(10.03)	11.18(10.97)
$\tilde{D}$					11.02(10.01)	11.44(10.93)
$\tilde{E}$						11.17(10.86)

The peak energies of Fig. 2(a), compiled in Table II, are in good accord with the data from laboratory and astronomical measurements [3–6,11]. In compiling the data the origin band is placed at 690.90 nm. A decreasing intensity pattern with increasing energy as noted in the spectrum of star Cernis 52 also follows from Fig. 2(a). To this end, we state that the present theoretical results unambiguously support the assignments of the three new DIBs to the electronic transitions in NP^+. This also convincingly adds to the present consensus and hypothesis that the PAH radical cations are potential carriers of DIBs.

We note that the $\tilde{B}$ band of NP^+ has also been recorded in matrix environments [3,6,22] and solvent induced redshifts of spectral lines were observed. The sharp vibronic lines in the alkyl halide matrix [22] turn diffuse in the Ne matrix [3,6]. In the latter, individual peak shifts in energy by ~0.5% and peak width increases by a factor of 4 to 5 times the gas phase value. Peak energies recorded in the Ne matrix [3] are given in Table II.

The $\tilde{B}$ band of AN^+ is presented along with experimental data [10] in Fig. 2(b). While its direct connection to the DIBs is sketchy, the following interesting correlations can be made. Vertically, the $\tilde{A}$ and $\tilde{B}$ states of AN^+ are energetically closer than in NP^+ (~0.62 eV vs ~1.62 eV). The spacing between the $\tilde{B}$ and $\tilde{C}$ states is nearly the same (~1.2 eV) in both. The energetic minimum of $\tilde{A}$-$\tilde{B}$ CIs in AN^+ occurs ~0.1 eV (~ 0.48 eV in NP^+) above the $\tilde{B}$ state minimum (cf. Table I). The minimum of the $\tilde{B}$-$\tilde{C}$ CIs in AN^+, however, occurs at higher energy compared to that in NP^+ (~3.79 vs ~2.01 eV relative to the $\tilde{B}$ state minimum). The coupling strengths of the b_{1u} vibrational modes between $\tilde{A}$-$\tilde{B}$ states are nearly the same in the two. Therefore, the close proximity of $\tilde{B}$ state minimum to the minimum of $\tilde{A}$-$\tilde{B}$ CIs causes stronger nonadiabatic effects in AN^+. This results in a huge density of vibronic lines [cf. bottom panel of Fig. 2(a)] and broadening of its $\tilde{B}$ band. The results reveal progressions of ~397 cm^{-1} and ~1331 cm^{-1} a_g vibrations.

Figure 3 displays the time dependence of electronic populations during the dynamical evolution of the $\tilde{B}$ state of NP^+ [panel (a)] and AN^+ [panel (b)]. The initial decline of the $\tilde{B}$state population in Fig. 3(a) relates to a decay rate of ~213 fs, in good accord with the experimental data of ~212 fs [6] and ~200 fs [7]. Because of strong coupling of the $\tilde{B}$ with the $\tilde{A}$ state and the latter with the $\tilde{X}$ state, population rapidly flows to the latter two states of NP^+. The CIs of $\tilde{B}$ state with the $\tilde{C}$-$\tilde{D}$-$\tilde{E}$ states occur at higher energy and therefore no noticeable population flows to the latter states in the present time scale. The situation is analogous in AN^+ except that a faster decay rate of ~30 fs of its $\tilde{B}$ state follows from Fig. 3(b), in good accord with an experimental prediction of <50 fs [7]. Occurrence of $\tilde{A}$-$\tilde{B}$ CIs much closer to the $\tilde{B}$ state minimum (cf., Table I) causes such a rapid decay.

To this end, we mention that much faster decay rates, viz., ~20 fs (~225 fs), ~60 fs (experimental value

TABLE II. Calculated vibronic energy levels of the $\tilde{B}$ state of NP^+ along with the various experimental results. Energies are given in nm.

Theory (present)	DIBs [11]	Pino *et al.* [4]	Bienner *et al.* [6]	Romanini *et al.* [5]	Salama *et al.* [3]
670.69 (0-0 peak)	670.74	670.69	670.70	670.65	674.1
648.15	648.87	648.93	648.89	648.84	652.0
637.49	⋯	638.57	⋯	⋯	⋯
⋯	⋯	634.72	⋯	⋯	⋯
627.07	⋯	628.50	⋯	⋯	⋯
617.09	⋯	617.34	⋯	⋯	⋯
609.87	611.80	612.48	612.52	⋯	615.1
607.55	⋯	609.27	⋯	⋯	⋯
⋯	⋯	597.33	⋯	⋯	⋯
591.17	⋯	593.40	593.35	⋯	596.5
588.78	⋯	591.36	⋯	⋯	⋯
582.29	⋯	585.27	⋯	⋯	⋯

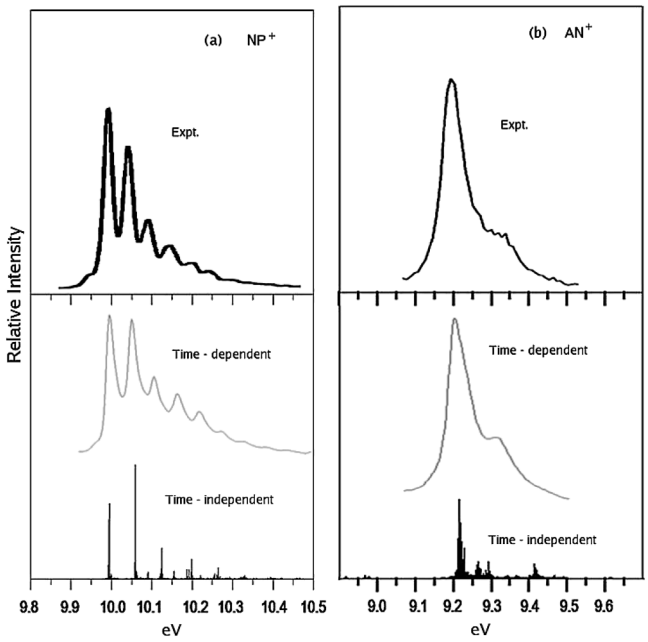

FIG. 2. The theoretical and experimental vibronic structures of $\tilde{B}$ state of NP^+ [panel (a)] and AN^+ [panel (b)].

~58 fs [4]) (>330 fs), ~29 fs (~38 fs), and ~15 fs (~89 fs) for the $\tilde{A}$, $\tilde{C}$, $\tilde{D}$, and $\tilde{E}$ state, respectively, are estimated for NP^+ (AN^+). The rapid nonradiative transfer of electronic population through multiple CIs quenches the fluorescence emission and underlies the mechanism of photostability of NP^+. In both NP^+ and AN^+ the $\tilde{C}$ state decays via $\tilde{C}$-$\tilde{E}$ and $\tilde{E}$-$\tilde{B}$ CIs (cf. Fig. 1). In AN^+ these intersections are energetically higher (cf., Table I), not readily accessible to the WP launched on the $\tilde{C}$ state which explains its longer decay rate.

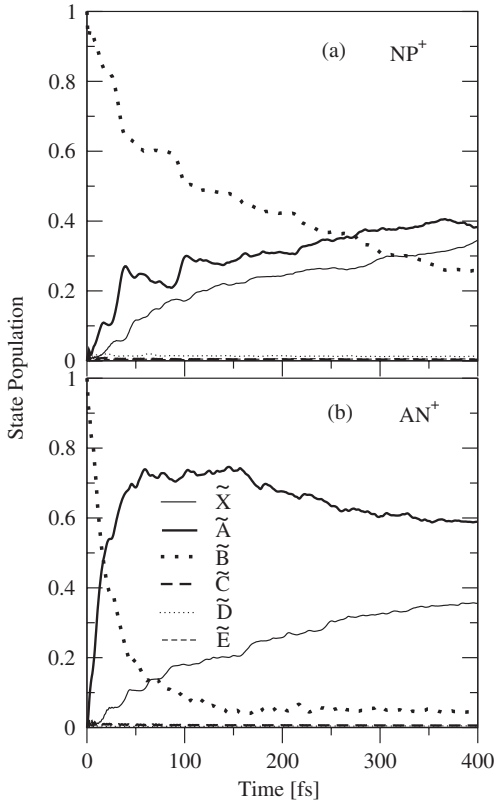

FIG. 3. Diabatic electronic populations during the dynamical evolution of the $\tilde{B}$ state of NP^+ [panel (a)] and AN^+ [panel (b)]. The population curve of a given state is identified in panel (b).

In conclusion, we have attempted to unravel some contentious issues of interstellar physics by performing *ab initio* quantum dynamical studies on two lowest radical cations of the PAH family. The outcomes unambiguously qualify PAHs as potential DIB carriers and a nonradiative deactivation of their excited electronic states is mediated by numerous complex nonadiabatic paths, which establishes the mechanism of their photostability. The theoretical results presented here complement for the first time the observations by astronomers as well as laboratory experimentalists. The present study is hoped to trigger further experimental and theoretical research in this area.

This study is supported in part by a research grant from the Department of Science and Technology (DST), New Delhi; Grant No. DST/SF/04/2006.

*smsc@uohyd.ernet.in

[1] *The Diffuse Interstellar Bands*, edited by A. G. G. M. Tielens and T. P. Snow (Kluwer Academic, Dordrecht, 1995).
[2] F. Salama *et al.*, Astrophys. J. **526**, 265 (1999).
[3] F. Salama and J. Allamandola, J. Chem. Phys. **94**, 6964 (1991).
[4] T. Pino, N. Boudin, and P. Bréchignac, J. Chem. Phys. **111**, 7337 (1999).
[5] D. Romanini *et al.*, Chem. Phys. Lett. **303**, 165 (1999).
[6] L. Biennier *et al.*, J. Chem. Phys. **118**, 7863 (2003).
[7] L. Zhao *et al.*, J. Phys. Chem. A **108**, 25 (2004).
[8] O. Sukhorukov *et al.*, Chem. Phys. Lett. **386**, 259 (2004).
[9] D. A. da Silva Filho *et al.*, Chem. Commun. (Cambridge) 15 (2004) 1702.
[10] R. S. Sanchez-Carrera *et al.*, J. Phys. Chem. B **110**, 18 904 (2006).
[11] S. Iglesias-Groth *et al.*, Astrophys. J. **685**, L55 (2008).
[12] K. F. Hall *et al.*, J. Phys. Chem. A **110**, 13591 (2006).
[13] V. S. Reddy and S. Mahapatra, J. Chem. Phys. **128**, 091104 (2008).
[14] M. Born and R. Oppenheimer, Ann. Phys. (Leipzig) **84**, 457 (1927).
[15] H. Köppel, W. Domcke, and L. S. Cederbaum, Adv. Chem. Phys. **57**, 59 (1984).
[16] M. H. Beck *et al.*, Phys. Rep. **324**, 1 (2000); G. A. Worth *et al.*, The MCTDH Package, Version 8.2 (2000).
[17] L. S. Cederbaum *et al.*, Chem. Phys. **26**, 169 (1977).
[18] B. N. Papas, M. S. Schuurman, and D. R. Yarkony, J. Chem. Phys. **130**, 064306 (2009).
[19] *Conical Intersections*, edited by W. Domcke, D. R. Yarkony, and H. Köppel (World Scientific, NJ, 2004), Vol. 15. See, for example, Chaps. 7, 10, 14, 16.
[20] L. S. Cederbaum, J. Phys. B **8**, 290 (1975).
[21] M. J. Frisch *et al.*, *Gaussian 03, Revision B. 05* (Gaussian, Inc., Pittsburgh, PA, 2003).
[22] T. Shida and S. Iwata, J. Am. Chem. Soc. **95**, 3473 (1973).